A Raman and Computational Study of Two Dithienyl Naphthodithiophenes: Synthesis and Characterization of New Polymers Showing Low Band Gap Optical and Electroactive Features

Juan Casado, J. Joaquín Quirante, Víctor Hernández, and Juan T. López Navarrete*
Departamento de Química Física, Facultad de Ciencias, Universidad de Málaga, 29071-Málaga, Spain

Kazuo Takimiya and Tetsuo Otsubo
Department of Applied Chemistry, Graduate School of Engineering, Hiroshima University, Higashi-Hiroshima 739-8527, Japan

Received: February 9, 2004

Two isomeric dithienyl naphthodithiophenes and their corresponding polymers have been thoroughly studied by using a combination of spectroscopic, electrochemical, and quantum chemistry techniques. The change between the syn and anti configuration of the sulfur atoms of the core translates into important differences in their optical and electrochemical properties. This study reveals the existence in the syn isomer of a bonding interaction, while in the anti isomer there exists a more delocalized π-electron distribution. The full assignment of the Raman spectra of the monomers has allowed to interpret, assign, and correlate the spectra of the polymers. Upon polymerization the Raman data indicate an increment of the bond length relaxation pattern for the electronic structure of the polymer regarding the monomers. The two polymers are surprisingly strong amphoters, showing very stable oxidation and reduction waves at relatively low potentials at the same time that they behave as low band gap polymers. From a material point of view, these polymers are very interesting substrates for electrically active layers with relevant photophysical properties.

I. Introduction

Conjugated organic molecules, either polymers or oligomers, likely constitute one of the greatest challenging fields of research regarding their applications in technological devices. Main applications, such as light emitting diodes,[1−5] solar cells, or electronic transistors (field-effect transistors), are presently being actively investigated.[5−9] In the field of electronics it is desirable to synthesize compounds that could behave as hole- and as electron-transporting materials, ambipolar systems, only by changing the gate potential which, without a doubt, will benefit and improve the realization of p−n semiconductors for electronic circuits. Regarding the light emitting diodes or their counterparts solar cell devices, the design of new conjugated polymers is directed toward the field of low band gap polymers, so-called to the conjugated polymers, with band gaps lower than 1.8 eV.

Particularly, systems derived from thiophene are very attractive since they favor the occurrence of highly extended π−electron conjugated compounds.[10−13] Recently, some of us have synthesized two isomeric dithienyl-substituted naphthodithiophene monomers that represent new types of heteroarene polyconjugated molecules which combine properties of fused carbon−carbon six-member rings (their cores are isoelectronic with pyrene) with the electronic properties of oligothiophenes.[14] Using the strategy of the introduction of two thiophene rings into the fused skeleton, their aromatic character seems to be greatly reduced. Moreover, it is somewhat intriguing that only by changing the configuration, syn or anti, of the two inner sulfur atoms of the monomers the molecular properties drastically change. As an example, the lowest energy band (π−π* band) is red shifted in the anti relative to the syn isomer by 75 nm (519 nm versus 444 nm). We call the attention of the reader to this fact because, for example, the red shift of the π−π* band on passing from bithiophene to sexithiophene is only around 100 nm.[10] It is worth mentioning that these two isomeric monomers have been implemented in organic field-effect transistors resulting that the sublimed film of the anti isomer well behaved as a p-channel semiconductor (μ_{FET} = (2−3) × 10^{-4} cm^2 V^{-1} s^{-1}), whereas the syn device did not work.[15]

In the field of materials science, band structure engineering has become important because the band gap is one of the most important factors of controlling physical properties. The discovery of polybenzo[*c*]thiophene,[16] whose band gap is 1.1 eV, that is, about 1 eV lower than that of polythiophene, opened the strategy of tuning the band gap by structural modification. There exist several powerful approaches on the construction of low band gap polymers. One strategy is the co-polymerization of aromatic and pro-quinoidal or quinoidal units, indicating that the combination of monomer segments with different electronic structures can lower the band gap through the relaxation of the bond length alternation pattern.[17] Another is the alternation of electron-donating and electron-accepting moieties giving rise to intrachain charge transfer that effectively reduces the energy gap.[18] Considering that the modification of the peri-fused core greatly reduces the aromatic character of these derivatives, one can reasonably think that their polymerization could yield low or very low band gap polymers with certain dependence with the type of configuration.

The development of such compounds, either short well-structured molecules or polymers, critically depends on the good understanding of the relationships between their structure and

* Corresponding author. E-mail: teodomiro@uma.es.

10.1021/jp040110i CCC: $27.50
Published on Web 05/15/2004

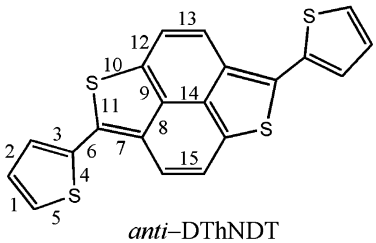

anti–DThNDT

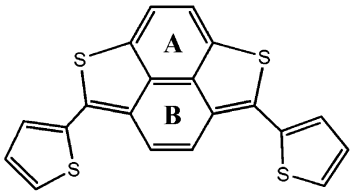

syn–DThNDT

Figure 1. Chemical structure for *syn*-DThNDT and *anti*-DThNDT. Bond numbering corresponds to that used in Table 1. A and B denote the two different six-membered rings.

physical properties. In this contribution, we describe investigations of the spectral and electrochemical properties of two monomers and their polymers to examine the structure−property correlation. To explore this relationship, we combine spectroscopic tools, UV−visible and Raman spectroscopies, electrochemical methods, and quantum chemical calculations. Most times structural studies on polymeric samples become extremely difficult by using conventional experimental techniques due to the inherent intractability, very low solubility, or structural disorder. However, in these cases Raman spectroscopy has shown to be particularly adequate and useful to record well-resolved scattering spectra which, by means of the correlation of the Raman bands of the monomer with those of the polymer, provides a method to follow structural changes upon polymerization. The computation of the Raman spectra of the monomers facilitates the measure of microscopic probes of the structure such as the vibrational normal modes through the precise assignment of their experimental bands.

II. Experimental and Theoretical Details

The chemical structures of 2,6-di(2-thienyl) naphtho[1,8-bc: 5,4-b′c′]dithiophene (*anti*-DThNDT) and 2,5-di(2-thienyl) naphtha-[1,8-bc: 5,4-b′c′]dithiophene (*syn*-DThNDT) are depicted in Figure 1.[14] Their iodine complexes were prepared in 1,2-dichloromethane by adding stoichiometric amounts and stirring the mixture for 3 h at room temperature. For the electrochemical polymerization, saturated solutions of the two dithienyl naphthodithiophenes were prepared in acetonitrile using tetrabutylammonium perchlorate as solid electrolyte in a 0.1 M concentration. Either a Pt disk of 1×1 cm^2 area or an ITO electrode was used as a working electrode in which the polymer is deposited. A Pt disk and an Ag/AgCl electrode were used respectively as auxiliary and as reference. The polymerization was carried out in cyclic voltammetry conditions between 0 and 1 V at 25 °C. For full electrochemical characterization of the polymers, saturated solutions of the monomer were replaced by freshly prepared solutions of the electrolyte.

The FT-NIR electron absorption spectra and the FT-Raman spectra were collected with a Bruker Equinox 55 FT-IR either using the FT-NIR mode with a Germanium detector working at room temperature or its FT-Raman accessory kit (FRA/106-S) with a Nd: YAG laser at 1064 nm. Each FT-NIR spectrum was obtained upon averaging 50 spectra, while particular conditions of the FT-Raman experiments were 50−100 mW of laser power and 1000−3000 scans with a spectral resolution of 2 cm^{-1} were averaged. The FT-Raman spectra of the polymers were obtained upon radiation of the Pt disk containing the electrochemically deposited material.

Geometry optimizations, molecular orbital topologies, and Raman spectra were calculated at the density functional theory (DFT)[19,20] level using the Becke's three parameter B3LYP exchange-correlation functional[21] and the 6-31G** basis set.[22] Calculations were performed on isolated entities in vacuum. Vertical electronic excitation energies were computed by using the time-dependent density functional theory (TDDFT).[23] Numerical applications reported so far indicate that TDDFT employing current exchange-correlation functional performs significantly better than HF-based single excitation theories for the low-lying valence excited states. It has been demonstrated that the vibrational spectra calculated with the DFT methodology satisfactorily agree with experimental spectra both in relative intensities and peak positions.[19] Since calculated vibrational spectra systematically overestimate frequency values due to electron correlation effects and basis set deficiencies, they must be properly corrected after inclusion of a uniform scaling factor of 0.96, as recommended by Scott and Radom.[20] All quoted theoretical vibrational frequencies reported along the paper are thus scaled values. All the calculations were performed using the A.7 revision of the Gaussian 98 program package running on an SGI Origin 2000 computer.[24]

III. Results and Discussion

(a) Optical Spectra, Electrochemistry, and Molecular Orbital Calculations of the Monomers. The experimental UV−vis absorption spectra of the two isomers nicely compare with the results obtained for the adiabatic vertical excitations calculated by the TDDFT/B3LYP/6-31G** method. The lowest energy and strongest band of the electronic absorption spectrum of *syn*-DThNDT in THF is measured at 444 nm (2.793 eV) with a extinction coefficient of 4.53. This transition corresponds to the excitation to the first excited electronic state and implies a one-electron promotion from the highest occupied molecular orbital (HOMO) to the lowest unoccupied molecular orbital (LUMO), which is calculated at 2.696 eV with an oscillator strength of 0.91. For the *anti*-DThNDT isomer, the lowest energy and strongest band of its UV−vis absorption spectrum in THF is measured at 519 nm (2.389 eV) with a extinction coefficient of 4.57 corresponding also with a one-electron promotion from the HOMO to the LUMO calculated at 2.292 eV with an oscillator strength of 0.80. Regarding the UV−vis data for *syn*-NDT and *anti*-NDT, which are the same systems without terminal thiophene rings, the lowest energy and strongest bands are experimentally measured, respectively, at 353 nm and at 417 nm, revealing thus how the outermost thiophene rings importantly interact with the core.

Figure 2 shows the atomic orbital composition calculated for the HOMO and the LUMO molecular orbitals of *syn*-DThNDT, *anti*-DThNDT, *syn*-NDT, and *anti*-NDT. First observation is that the HOMO and LUMO have different eigenvectors depending on the syn or anti configuration, which is particularly noticeable at the level of the core; as an example, one can observe that the HOMO of the anti molecules have more nodal planes than their syn counterparts. Qualitatively, the topologies of the orbitals are of π-nature and extend over the whole structure, although the HOMO of the *syn*-DThNDT is apparently more concentrated or localized in the core while for the *anti*-DThNDT the HOMO is more uniformly distributed. As a

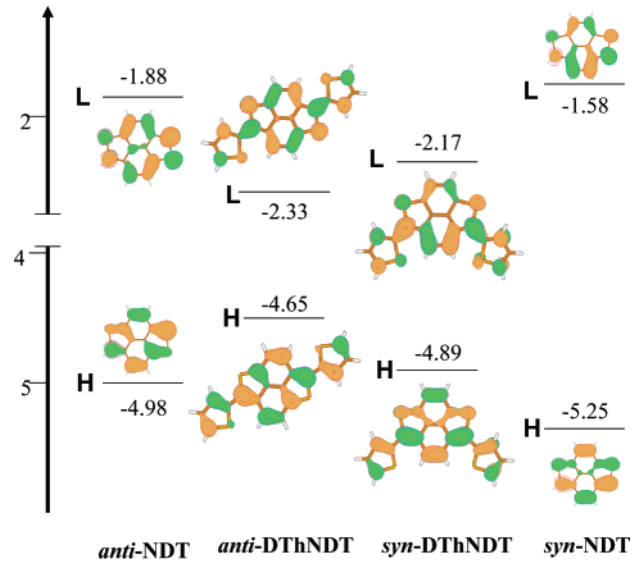

Figure 2. HOMO (H) and LUMO (L) orbitals for *syn*-DThNDT, *anti*-DThNDT, *syn*-NDT, and *anti*-NDT. Absolute energies values (in eV) are also shown.

consequence of the effective delocalization of the two molecular orbitals over the entire structure, one must expect significant changes in energies on going from the NDT to the DThNDT isomers. Only for the HOMO orbital of the *syn*-DThNDT molecule (and in *syn*-NDT), and judging from the same character of the phase of the atomic orbitals located between the two inner suphur atoms, does there exist a bonding interaction that is likely responsible of the stabilization of the HOMO and the subsequent destabilization of the LUMO turning out in a larger energy gap for the syn isomer. As a consequence, the maximum of the $\pi-\pi^*$ band, in the case of the *anti*-NDT regarding its *syn*-NDT counterpart, is red shifted by 64 nm and by 75 nm in the case of the DThNDT isomers.

Figure 2 also shows the values for the absolute energies corresponding to the HOMO and LUMO orbitals for the molecules under analysis. Also here the bonding interaction that causes a net energetic stabilization of 0.24 eV of the *syn*-DThNDT HOMO (absolute calculated energy of −4.89 eV) with respect to the *anti*-DThNDT HOMO (absolute calculated energy of −4.65 eV) nicely addresses the experimental finding that the first one-electron extraction in the syn isomer aproximately requires 0.27 V more than the first one-electron extraction in the anti isomer: 0.62 V in *anti*-DThNDT and 0.89 V in *syn*-DThNDT.[14] However, the differences between the first oxidation peak potentials in the NDT homologues are much smaller, only 0.08 V (1.01 V for *syn*-NDT and 0.93 V for *anti*-NDT), than those cited for the DThNDT isomers, which could be explained in terms of the better delocalization of the injected positive charge in a system with two more thiophene rings.

To address this last item, let us have a look at the calculated B3LYP/6-31G** total atomic charges for both isomers as displayed in Figure 3. Each of the two innermost sulfur atoms supports a total charge of +0.245 *e* in *syn*-DThNDT and of + 0.266 e in *anti*-DThNDT, which are balanced by the α-carbon atoms directly connected to them that bear a net charge of −0.159 *e* in *syn*-DThNDT and of −0.172 e in *anti*-DThNDT. Moreover, such charge reorganization affects the whole A ring, which supports a net charge of −0.510 *e* against −0.280 *e* for each aromatic ring in the naphthalene-like moiety of *anti*-DThNDT. This charge analysis illustrates the variations on the one-electron oxidation potentials in the sense that in the *syn*-DThNDT isomer the electron extraction should be more localized, as opposed to the *anti*-DThNDT case in which the injected positive charge could be shared by the whole system.

(b) Optimized Molecular Geometries. The crystalline structure of *anti*-DThNDT has already been resolved; however, no data for the *syn*-DThNDT are available.[14] Table 1 compares the experimental bond lengths obtained from the X-ray study and those calculated with the DFT/B3LYP/6-31G** methodology for the *anti*-DThNDT molecule. The mean value of the differences between the X-ray and the calculated bond lengths is 0.017 Å, and a good accordance between the experiment and theory is noticed. Figure 3 summarizes all the B3LYP/6-31G** optimized bond distances for both compounds considered as isolated entities in the vacuum.

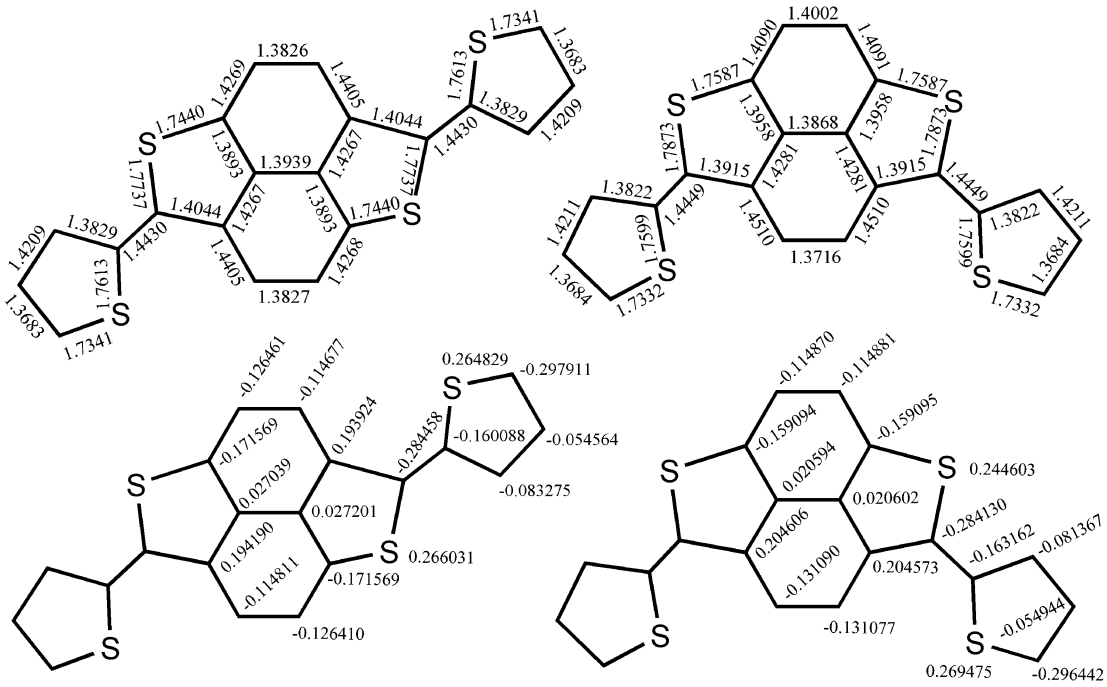

Figure 3. B3LYP/6-31G** optimized bond lengths lengths in Å and total Mülliken atomic charges for *syn*-DThNDT and *anti*-DThNDT.

TABLE 1: Experimental and B3LYP/6-31G Theoretical C−C and C−S Bond Lengths (in Å) for the for *anti*-DThNDT[a]**

bond number	exp.	theor.	bond number	exp.	theor.	bond number	exp.	theor.
1	1.32(1)	1.3683	6	1.447(9)	1.4430	11	1.762(7)	1.7737
2	1.43(1)	1.4209	7	1.391(9)	1.4044	12	1.422(9)	1.4269
3	1.417(9)	1.3829	8	1.426(9)	1.4267	13	1.373(9)	1.3826
4	1.711(7)	1.7613	9	1.376(9)	1.3893	14	1.40(1)	1.3939
5	1.682(8)	1.7341	10	1.735(7)	1.7440	15	1.373(9)	1.3827

[a] Bond numbering corresponds to that appearing in Figure 1. Experimental data are taken from ref 14.

The molecular structures of *anti*-DThNDT and *syn*-DThNDT are nearly planar, even including the two outermost thiophene rings that are only slightly deviated by around 6° from the coplanarity of the core. The analysis of both peri-fused moieties reveals some differences despite that they are completely planar and isoelectronic. Let us employ the concept of the mean of the differences between the consecutive single-double carbon−carbon bond lengths (BLA) as a tool to comparatively evaluate the relaxation of the bond length alternation pattern in the two molecules. Furthermore, to analyze the aromaticity of the molecules, we will make use of the nucleus-independent chemical shift (NICS), which is defined as the negative of the magnetic shielding at some selected point in space, e.g., at a ring center.[25,26] Positive and negative NICS values indicate paratropicity and diatropicity, respectively, and hence have been referred to as indicators of local aromatic character. In the *syn*-DThNDT isomer, the BLA for the six-member ring denoted as B in Figure 1 is 0.0479 Å, which is the largest BLA among the six- or five-member rings of the two molecules, while its NICS value, +1.9, denotes the anti-aromatic character of this ring. However, the six-member ring denoted as A in Figure 1, mostly affected by the bonding interaction, has a BLA value of 0.0104 Å and NICS data of −7.3, which is relatively close to that of benzene, −9.7.[25] The BLAs for the two six-member rings in the *anti*-DThNDT are equal, accounting to be 0.0318 Å, while their NICS values amount to −2.28 (NICS of naphthalene are −9.9), thus showing a intermediate aromaticity between those six-member rings of *syn*-DThNDT. The BLA values of the two innermost thiophene rings in *syn*-DThNDT are 0.0344 Å, which compare with the BLA values of the corresponding thienyl rings in the *anti*-DThNDT, 0.0298 Å. These data indicate an apparent benzenoidization of the A ring versus a naphthaleidization of the two six-member rings in *anti*-DThNDT.

Let us now compare some specific bond distances such as the length of the central CC bonds (those shared by the two six-member rings), 1.3868 Å in *syn*-DThNDT and 1.3929 Å in *anti*-DThNDT, which could be related to the bonding interaction that affects this part of the syn isomer. Also, the CC bond lengths of the thiophene affected by such interaction are shorter than those that are not involved, resulting in a distorted thiophene ring. This distortion could give rise to a localization or pinning of the π-electrons in this molecular domain at the expenses of the loss of aromatic character of the thiophenes. The same reason applies to the C−S bonds whose bond lengths are 1.7587 Å, 0.0286 Å shorter than the C−S bonds of the outer thiophene rings, which can be considered as typical aromatic thiophenes.

The overall electronic structure of the *anti*-DThNDT molecule can be considered as a result of the competitive effect between two extreme resonance structures: one is aromatic for its thiophene rings, while in the other a naphthalene moiety can be drawn for the two six-member rings; consequently, the naphthalenic structure arises at the expenses of the quinoidization of the two inner thiophenes. As it will be discussed later, the stabilization of the radical anion species of *anti*-DThNDT is mainly due to the gaining of aromatic character of the two six-member rings, whereas for the radical cation, the quinoidization of the thienyl part is the driving force for its generation. From this point of view, the naphthalene-like moiety can be regarded as an electron-acceptor as compared to the thienyl part which seems to behave as an electron-donor. Furthermore, the ground electronic state of *anti*-DThNDT could partially consist of an apparent charge transfer from one to another, therefore explaining the significant red shift of its $\pi-\pi^*$ band. This electronic effect could be more pronounced in the case of the *anti*-DThNDT-based polymer since the thienyl part increases its contribution through the generation of a bithiophene between the peri-fused cores.

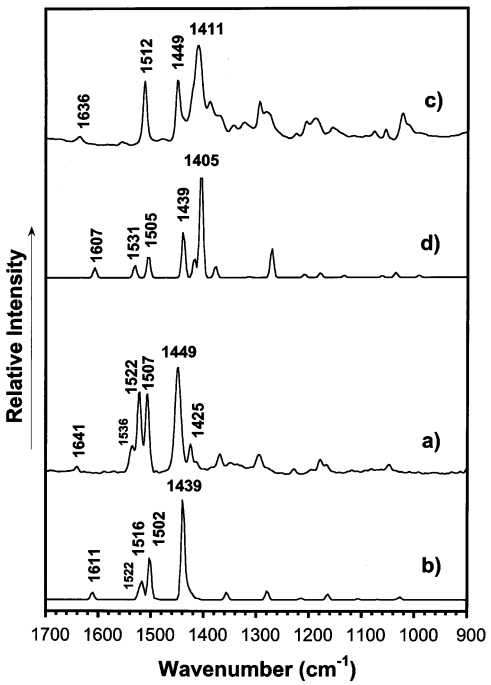

Figure 4. Comparison between the experimental and theoretical B3LYP/6-31G** Raman spectra of *syn*-DThNDT (a and b, respectively) and of *anti*-DThNDT (c and d, respectively).

(c) Raman Spectra of the Thienyl Naphthadithiophenes. Figure 4 displays the FT-Raman spectra of *syn*-DThNDT and *anti*-DThNDT together with their corresponding theoretical B3LYP/6-31G** spectra revealing a good matching, both in intensity and peak positions, between experimental results and theoretical calculations. Table 2 summarizes the wavenumber and the assignment of the main Raman bands of the compounds studied here. The theoretical frequencies are only overestimated by a relative amount, 4−5% or by 25−30 cm^{-1} in absolute values for the bands around 1500 cm^{-1}. The agreement between the experimental and simulated vibrational spectra better supports the reliability of the calculations as a source of information regarding the molecular properties.

The Raman spectra of *syn*-DThNDT and *anti*-DThNDT show a relatively low number of bands, thus only 4−5 intense scatterings are observed despite that theory predicts the existence

TABLE 2: Wavenumber Values, Correlation, and Assignments of the Main Raman Bands for *syn*-DThNDT, *anti*-DThNDT, poly(*anti*-DThNDT), and poly(*syn*-DThNDT) in Their Neutral States as Solids

syn-DThNDT	*syn*-DThNDT-I_2	*anti*-DThNDT	*anti*-DThNDT-I_2	poly(*syn*-DThNDT)	p-doped poly(*syn*-DThNDT)	poly(*anti*-DThNDT)	p-doped poly(*anti*-DThNDT)
1641	1638	1636		1639	1639		
		1553					
1536							1518
1522		1512				1510	1502
1507							
	1485	1479		1491	1485		
1449		1449				1448	1443
1425						1429	
		1411		1406	1400	1400	1390
	1394	1389	1383				
1369		1344					1357
	1310	1323					1303
1295		1294	1291	1300	1307	1293	
		1282	1275				1265
1228		1225	1230	1220			1233
		1205					1214
1179	1185	1188	1178	1182	1187		1177
	1144	1156				1152	
	1112		1107				
	1081	1076			1073	1093	1071
1049	1054	1055	1052	1053		1051	
		1023	1020	1022	1020	1024	1020
900	908			905	909		

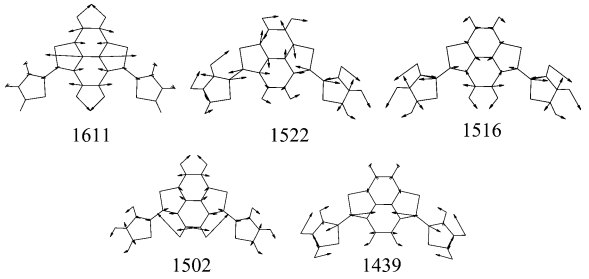

Figure 5. Eigenvectors associated with the most important theoretical Raman bands of *syn*-DThNDT. Wavenumber data, in cm^{-1}, correspond to scaled values.

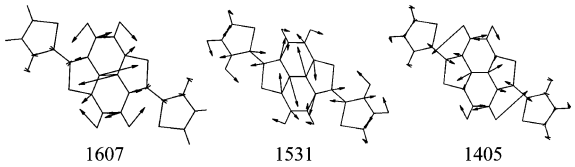

Figure 6. Eigenvectors associated with the most important theoretical Raman bands of *anti*-DThNDT. Wavenumber data, in cm^{-1}, correspond to scaled values.

of plenty of Raman-active vibrations (70 for *anti*-DThNDT and 96 for *syn*-DThNDT). This apparent contradiction is accounted for by the existence for this class of polyconjugated molecules of an effective electron−phonon coupling between the electronic structure and some particular skeletal vibrations which are very much enhanced.[27,28] As a consequence, only some totally symmetric modes are selectively intensified, while the rest of the totally symmetric modes and the nontotally active symmetric Raman modes become weak or almost undetectable.

The following vibrations are of particular importance to extract relevant information in our systems. (i) the experimental dispersion at 1636 cm^{-1} in *anti*-DThNDT (calculated at 1607 cm^{-1}) correlates with the line observed at 1641 cm^{-1} in *syn*-DThNDT (calculated at 1611 cm^{-1}). According to their eigenvectors in Figures 5 and 6, they can be described as stretching modes of the central CC bond common to the two six-member rings with contributions of the CC stretching and bending vibrations of the same six-member rings. As seen, this mode is almost exclusively located in the naphthalene-like moieties, which allows for comparison with their parent pyrene at 1643 cm^{-1} or at 1648 cm^{-1} in *syn*-NDT (spectra not shown). The progressive downshifting of this band could be a consequence of the softening of this bond due to an increased delocalized electron distribution. In this regard, the difference of 5 cm^{-1}, although small, between *anti*-DThNDT and *syn*-DThNDT isomers can be somewhat accounted for by the bonding interaction that particularly affects this part of the molecule. (ii) There exist intense Raman lines in the interval 1550−1500 cm^{-1} in the spectra of both thienyl naphthadithiophenes. At 1536, 1522, and 1507 cm^{-1} (theoretically calculated at 1522, 1516, and 1502 cm^{-1}) in *syn*-DThNDT which might be assigned to CC stretching modes but with unequal contributions. The former band mainly arises from the tetrathienyl spine, for the second one, the CC bonds of the outermost thiophene rings mostly vibrate, while the third scattering contains large CC motions of the naphthalene-like moiety (Figures 5 and 6). In this region only one Raman line at 1512 cm^{-1} is observed for *anti*-DThNDT, which is calculated at 1531 cm^{-1} and which corresponds to a CC stretching vibration highly delocalized over the whole molecule (all the CC bonds equally contribute). (iii) The most intense band of the Raman spectrum of the *syn*-DThNDT appears at 1449 cm^{-1} (calculated at 1439 cm^{-1}). The analysis of its associated eigenvector reveals that it arises from a stretching vibration with major contributions of the two side α,α' thiophenes. For *anti*-DThNDT, the strongest band is measured at 1411 cm^{-1} (calculated at 1405 cm^{-1}) and might be described as a CC stretching vibration mainly located in the core, although in this case the contributions of the rest of CC bond stretching are important. This line could correlate with the strongest band of pyrene at 1407 cm^{-1} corresponding to a CC stretching vibration delocalized over the entire molecule. Furthermore, the appearance of the strongest Raman band at low wavenumber values, 1411 cm^{-1} versus 1449 cm^{-1}, could also be a marker of the more pronounced relaxation of the bond length alternation pattern.

(d) Raman Spectra of the Molecular Complexes. These two isomers can be regarded as strong electron-donating compounds due to their high electron richness. In fact, they form

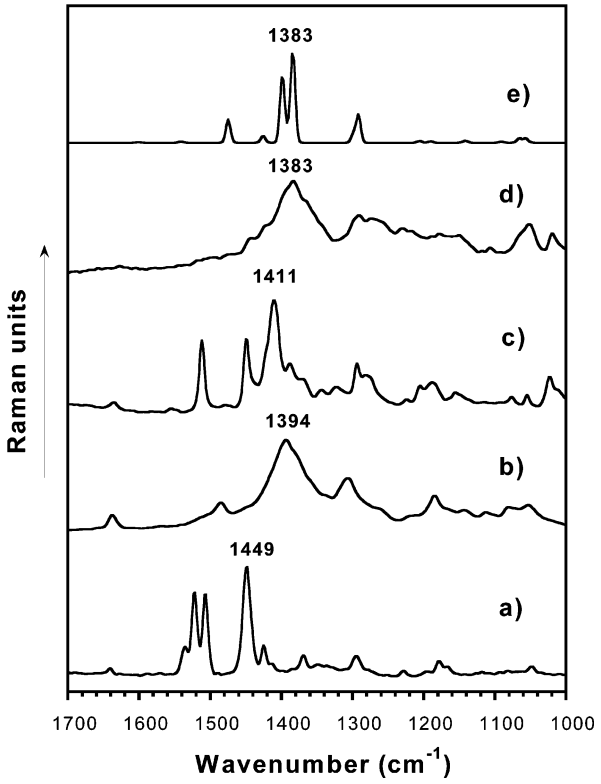

Figure 7. Comparison between the Raman spectra of (a) neutral *syn*-DThNDT, (b) iodine-treated *syn*-DThNDT, (c) neutral *anti*-DThNDT, and (d) iodine-treated *anti*-DThNDT. Spectrum (e) corresponds to that calculated at the B3LYP/6-31G** level for the radical cation of *anti*-DThNDT.

molecular complexes either with moderate or strong electron acceptors. Particularly, their iodine complexes have revealed to be very efficient conductors, reaching conductivity values of 6.3 and 10 Scm^{-1} respectively for *syn*-DThNDT and *anti*-DThNDT.[14] These complexes are black solids which strongly absorb in the NIR spectral region; therefore, their Raman spectra recorded with a excitation light at 1064 nm are taken in resonance Raman conditions, which underlines the fact that the Raman bands are exclusive features of the $\pi-\pi^*$ chromophore.

Figure 7 displays the FT-Raman spectra of the charged-transfer salts generated upon treatment with iodine. First observations are that no bands due to the neutral species are now observed and that the peaks of the new bands, relative to the neutral systems, are downshifted in accordance with the increment of the relaxation of the bond length alternation pattern due to electron extraction.

For *anti*-DThNDT-I_2, the most intense band appears as a structured band at 1383 cm^{-1} related to the strongest band in the neutral molecule at 1411 cm^{-1}. At higher wavenumbers the bands at 1442 cm^{-1} and 1421 cm^{-1} can correspond to vibrations of the thienyl moieties since there is good agreement with the characteristic Raman lines of the radical cations of linearly α,α′-linked oligothiophenes appearing at 1438 and 1417 cm^{-1}.[29] These two scatterings arise from typical vibrations of the quinoid structures in p-doped oligothiophenes which, in some sense, could invoke to the quinoidization of the thiophene rings of the isomer. The influence of the configuration change of the two inner thiophene rings is also noticed in the Raman spectrum of *syn*-DThNDT-I_2. Now the strongest bands are recorded at 1394 cm^{-1} and at 1307 cm^{-1}, whereas no quinoid bands arising from the thienyl moieties are measured around 1440 cm^{-1}. In contrast, a well-resolved peak appears at 1485 cm^{-1}, which is a typical wavenumber for the vibrations of aromatic C═C

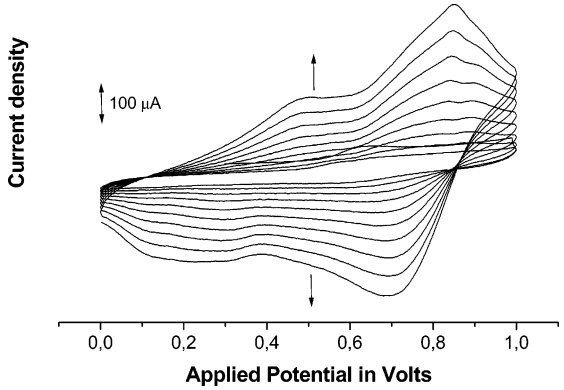

Figure 8. Repetitive cycling of a saturated solution of *anti*-DThNDT in acetonitrile 0.1 M $TBAClO_4$.

stretching of neutral linearly α,α′-linked oligothiophenes.[30] To theoretically explore the Raman spectra of these complexes, B3LYP/6-31G** calculations of the spectrum of the radical cation of *anti*-DThNDT have been carried out. This theoretical spectrum, which is shown in Figure 7, reproduces quite well the experimental features corresponding to the iodine-treated *anti*-DThNDT complex. For example, the strongest experimental band is measured at 1383 cm^{-1}, which results from the overlapping of various bands, and the strongest theoretical feature is also calculated at 1383 cm^{-1} with an intense band very close in frequency at 1393 which could justify the structured and broad feature of the experimental line. Also the theoretical bands at 1472 and 1427 cm^{-1} correlate respectively to the two observed bands at 1442 and at 1420 cm^{-1} in the spectrum of the iodine-treated *anti*-DThNDT complex. The nice matching between theory and experiment leads us to reasonably consider that the molecular complexes consist of the radical cation salts. Since these species are comparable with polarons in solid-state physics, it is quite intriguing to study and compare them with the analogues in the corresponding heavy p-doped polymers.

(e) Electrochemical and Raman Study of Low Band Gap Polymers. Application of recurrent potential scans of each monomer solution with a positive limit set at higher values than the first of the oxidation waves leads to the development of new redox processes at lower potentials. The current of these new processes continues to increase in intensity upon additional cycling, which is consistent with the deposition of an electroactive polymer onto the surface of the working electrode. Figure 8 shows this CV for the case of *anti*-DThNDT in which two seemingly reversible and broad waves at 0.38 and 0.76 V, corresponding to the successive oxidations of the resulting polymer, clearly appear. Further evidence for the formation of the polymer is the observation of a dark blue or green film on the surface of the working electrode, which is relatively highly stable under normal conditions. The surfaces of the polymers were clearly powdered. The two outermost α-positions of the dithienyl naphthodithiophenes are electrochemically reactive to readily effect polymerization under the cyclovoltammetric conditions.

The electrochemically polymerized films of each monomer, poly(*anti*-DThNDT*)* and poly(*syn*-DThNDT*)*, were thoroughly washed in acetonitrile to remove the excess monomer, and subsequent cyclic voltammetry was performed in monomer-free electrolyte. Figure 9 shows the CV for the poly(*anti*-DThNDT*)* which unexpectedly shows one irreversible process centered at −0.81 V in addition to the already-mentioned two oxidation processes. The occurrence of anodic and cathodic processes allows to measure the difference between the thresholds for the

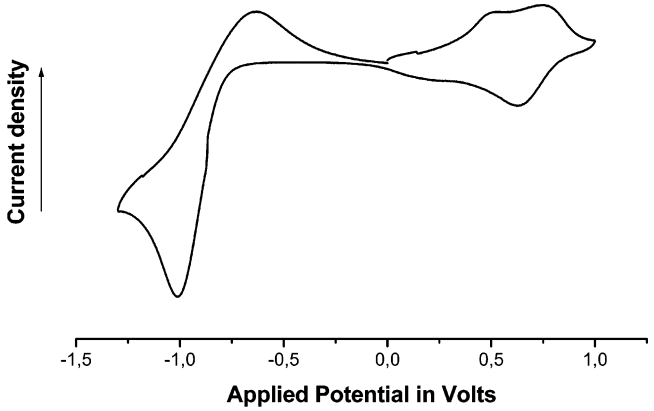

Figure 9. Cyclic volyametry of a poly(*anti*-DThNDT) film deposited in a Pt electrode in acetonitrile 0.1 M $TBAClO_4$.

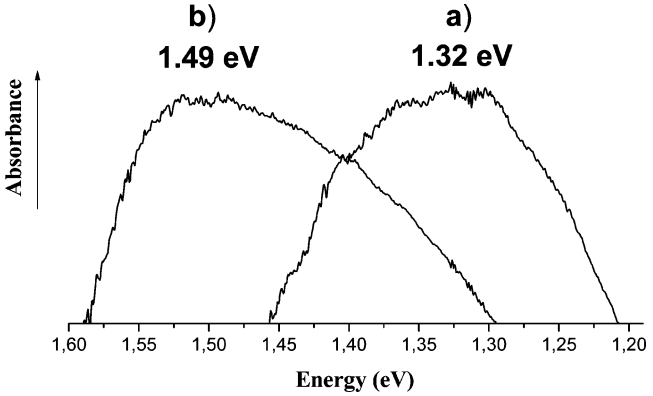

Figure 10. FT-NIR spectra of (a) neutral poly(*anti*-DThNDT), and (b) poly(syn-DThNDT) films deposited into an ITO electrode.

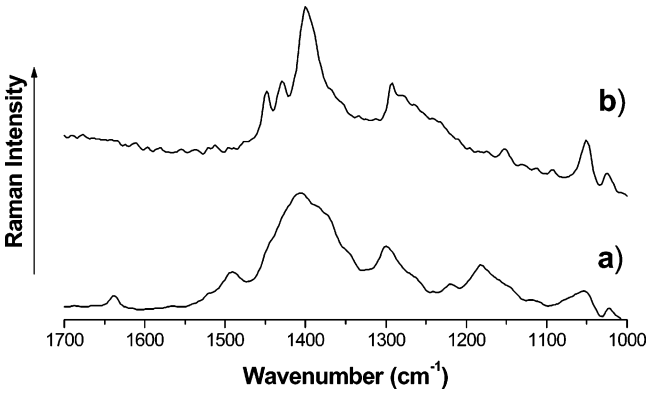

Figure 11. Comparison between the Raman spectra of (a) neutral poly(*syn*-DThNDT), and (b) neutral poly(*anti*-DThNDT) films.

oxidation wave (p-doping) and for the reduction wave (n-doping), electrochemical band gap, which account to be 1.19 V (1.57 V considering the second oxidation) in the range of the so-termed low band gap polymers. From another point of view, we must stress the existence of an amphoteric redox behavior for this system which is a key requirement for ambipolar transport in a given material. Poly(*syn*-DThNDT) also behaves as an amphoteric polymer, although both the oxidation and reduction waves take place at more energetic values (1.39 V for the first process and 1.68 V for the second one), resulting in a larger electrochemical band gap.

To theoretically justify this particular electrochemical behavior, calculations at the B3LYP/6-31G** level for the radical cation and radical anion species of *anti*-DThNDT have been carried out. After injection of one negative charge in *anti*-DThNDT, the more relevant structural change in the molecule consists of an increased naphthalene character of the two six-member rings. The new BLA calculated for this moiety is 0.0122 Å, which is considerably smaller than 0.0318 Å in the neutral monomer; furthermore, their NICS values become more negative than in the neutral species. The gain in aromatic character of this part of the molecule very much helps the energetic stabilization of the anion, addressing, in this way, the experimental appearance of n-doping in the polymer. In the case of the radical cation species, the BLA of this part is 0.0203 Å (also their NICS are slightly more negative than those of the neutral system), while the largest structural changes affect the outermost thiophene rings, since their BLAs amount to 0.0175 Å in the radical cation and 0.0298 Å in the neutral *anti*-DThNDT and 0.0351 Å in the radical anion. Consequently, the calculations apparently foresee the quinoidization of the thienyl rings as the relevant change in the structure that could energetically stabilize the injected positive charge and the appearance of p-doping.

The polymers were also obtained in an ITO electrode with the goal of obtaining their electronic spectra as shown in Figure 10. The energy values for the maxima of their low lying electronic transition ($\pi-\pi^*$ band) were measured at 1.32 eV in poly(*anti*-DThNDT) and at 1.49 eV in poly(*syn*-DThNDT), which are also characteristic of low band gap polymers. These optical values nicely correlate with the measured electrochemical band gap, thus an energy gap difference of around 0.2 eV is measured between both polymers either using optical or electrochemical techniques.

Figure 11 shows the FT-Raman spectra of the neutral poly(*anti*-DThNDT) and poly(*syn*-DThNDT) polymers. The main Raman band is downshifted by 11 cm^{-1} (1400 cm^{-1}) relative to the strongest line in the spectrum of the *anti*-DThNDT monomer as a consequence of the structural relaxation of the repetitive unit due to the increment of the π-electron delocalization in the polymer lattice. The line at 1448 cm^{-1} is only slightly affected regarding its monomer at 1449 cm^{-1}, while the new band at 1429 cm^{-1} must be assigned to a stretching vibration emerging from the new bithiophene moiety generated upon linking of the monomers. The wavenumber of this band correlates with the scattering at 1441 cm^{-1} in α,α'-bithiophene; therefore, the 12 cm^{-1} downshifting is likely due to conjugation with the peri-fused moieties. The spectrum of poly(*syn*-DThNDT) shows its strongest scattering at 1406 cm^{-1}, that is, at higher wavenumber than its anti homologue as a consequence of the already mentioned π-electron pinning in the peri-fused moiety. This is particularly clear for the band at 1639 cm^{-1} in the syn polymer measured at 1641 cm^{-1} in the monomer. Finally, the medium intensity Raman band at 1491 cm^{-1} of poly(*syn*-DThNDT) could be related to the bands in the monomer around 1510 cm^{-1}. Again, this frequency downshift is due to the structure relaxation upon polymerization.

Figure 12 displays the FT-Raman spectra of both polymers anodically treated at 0.9 V. The comparison of the spectrum of the radical cation salt of the *anti*-DThNDT with the Raman spectrum of heavily p-doped poly(*anti*-DThNDT) reveals a large resemblance both in peak position and in intensity. The similarities are particularly significant for the bands at 1390 (the strongest one), 1303, 1233, 1177, 1071, and at 1019 cm^{-1}, which correlate with the bands in iodine-treated *anti*-DThNDT at 1383 (the strongest one), 1291, 1230, 1178, 1052, and at 1019 cm^{-1}. The good matching is also valid in the case of the Raman spectrum of p-doped poly(*syn*-DThNDT) and that of the radical cation salt of its monomer. For instance, the bands at 1639, 1486, 1400, (the strongest one), 1307, 1187, and 1073 cm^{-1} in the doped polymer very well correlate with the bands at 1638,

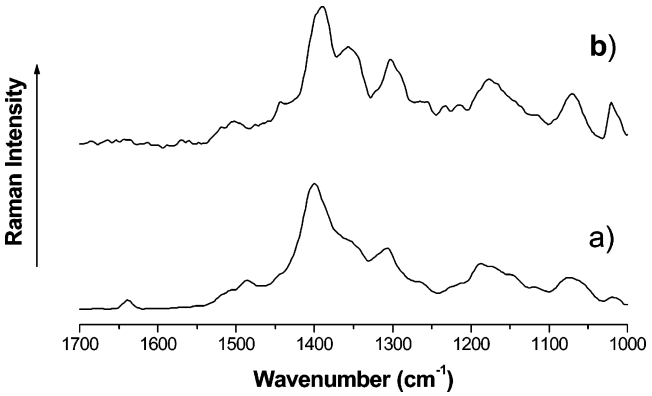

Figure 12. Comparison between the Raman spectra of (a) p-doped poly(*syn*-DThNDT), and (b) p-doped poly(*anti*-DThNDT) films.

1485, 1394, (the strongest one), 1307, 1185, and 1081−1053 cm^{-1} in *syn*-DThNDT-I_2.

IV. Summary and Conclusions

According to the strategy of incorporating heteroatoms into aromatic hydrocarbons for developing new advanced materials, two isomeric dithienyl naphthodithiophenes and their corresponding polymers have been thoroughly studied by using a combination of spectroscopic, electrochemical, and quantum chemistry techniques. The change between the *syn* or *anti* configuration of the sulfur atoms of the core for the monomers translates in important differences in their optical and electrochemical properties. This is due to the existence of the syn isomer of a bonding interaction extended between the two core sulfurs which causes a pinning of the π-electron in this molecular domain. For the *anti* isomer, there exists a more delocalized electronic distribution.

Monomers and polymers have been completely studied by means of Raman spectroscopy. The full assignment of the scattering spectra of the dithienyl naphthodithiophenes, with the help of density functional theory calculations, allows us to interpret, assign, and correlate the spectra of the polymers. Regarding the electronic structure, the generation of the polymer lattice causes an important increment of the bond length relaxation pattern relative to their building units as followed by the downshifting of almost all the Raman bands in the spectra of the polymers. Furthermore, the use of Raman spectroscopy has been revealed as a powerful tool for addressing the topic of the type of charge defects generated in the heavily p-doped polymers. From the comparison of the Raman spectra of the radical cation salts of the monomers with the Raman spectra of the oxidized polymers, we can conclude that the microscopic charge defects responsible for the conduction phenomena in these material likely are of polaronic character.

These polymers are surprisingly highly amphoteric, showing very stable oxidation and reduction waves at relatively low potential, which makes these samples potential candidates for ambipolar transport in electronic devices. Particularly for the poly(*anti*-DThNDT), the thresholds for the oxidation (p-doping) and for the reduction (n-doping) waves is 1.19 eV, which is in the range of the so-called low band gap polymers. From a material point of view, these polymers are very interesting substrates that could behave as electrically active layers at the same time that they show interesting photophysical and low energy absorbing features. It has to be stressed that efficient solar cells require the combination of light absorbing units with the ability of the material of easily transport the photogenerated charged separated states.

Acknowledgment. J.C. is grateful to the Ministerio de Ciencia y Tecnología of Spain for a Ramón y Cajal research position of Chemistry at the University of Málaga. The present work was supported in part by the Dirección General de Enseñanza Superior (DGES, MEC, Spain) through the research projects BQU2003-03194. We are also indebted to Junta de Andalucía (Spain), funding for our research group (FQM-0159).

References and Notes

(1) Tour, J. M. *Acc. Chem. Res.* **2000**, *33*, 791.

(2) Chen, J.; Reed, M. A.; Rawlett, A. M.; Tour, J. M. *Science* **2000**, *286*, 1550.

(3) Reed, M. A.; Zhou, C.; Muller, C. J.; Burgin, T. P.; Tour, J. M. *Science* **1997**, *278*, 252.

(4) Noda, T.; Shirota, Y. *J. Am. Chem. Soc.* **1998**, *120*, 9714.

(5) Noma, N.; Tsuzuki, T.; Shirota, Y. *Adv. Mater.* **1995**, *7*, 647. Katz, H. E.; Bao, Z.; Gilat, S. L. *Acc. Chem. Res.* **2001**, *34*, 359.

(6) Schön, J. H.; Berg, S.; Kloc, C.; Batlog, B. *Science* **2000**, *287*, 1022.

(7) Katz, H. E.; Bao, Z. *J. Phys. Chem. B* **2000**, *104*, 671.

(8) Granstrom, E. L.; Frisbie, C. D. *J. Phys. Chem. B* **2000**, *103*, 8842. Wold, D. J.; Frisbie, C. D. *J. Am. Chem. Soc.* **2000**, *122*, 2970.

(9) Pappenfus, T. M.; Chesterfield, R. J.; Frisbie, C. D.; Mann, K. R.; Casado, J.; Raff, J. D.; Miller, L. L. *J. Am. Chem. Soc.* **2002**, *124*, 4184.

(10) For example: Hotta, S.; Waragai, K. *J. Mater. Chem.* **1991**, *1*, 835.

(11) van Haare, J. A. E. H.; Havinga, E. E.; van Dongen, J. L. J.; Janssen, R. A. J.; Cornil, J.; Bredas, J. L. *Chem. Eur. J.* **1998**, *4*, 1509.

(12) Casado, J.; Miller, L. L.; Mann, K. R.; Pappenfus, T. M.; Higuchi, H.; Ortí, E.; Milián, B.; Pou-Amérigo, R.; Hernández, V.; López Navarrete, J. T. *J. Am. Chem. Soc.* **2002**, *124*, 12380.

(13) Casado, J.; Pappenfus, T. M.; Miller, L. L.; Mann, K. R.; Ortí, E.; Viruela, P.; Pou-Amérigo, R.; Hernández, V.; López Navarrete, J. T. *J. Am. Chem. Soc.* **2003**, *125*, 2524.

(14) Takimiya, K.; Kato, K.; Aso, Y.; Ogura, F.; Otsubo, T. *Bull. Chem. Soc. Jpn.* **2002**, *75*, 1795.

(15) Kunugi, Y.; Takimiya, K.; Yamashita, K.; Aso, Y.; Otsubo, T. *Chem. Lett.* **2002**, *10*, 958.

(16) Wudl, F.; Kobayashi, M.; Heeger, A. J. *J. Org. Chem.* **1984**, *49*, 3382. Kobayashi, M.; Colaneri, M.; Boysel, M.; Wudl, F.; Heeger, A. J. *J. Chem. Phys.* **1985**, *82*, 5717.

(17) Kürti, J.; Surján, P. R.; Kertesz, M. *J. Am. Chem. Soc.* **1991**, *113*, 9865. Kitamura, C.; Tanaka, S.; Yamashita, Y. *Chem. Mater.* **1996**, *8*, 570. Karikomi, M.; Kitamura, C.; Tanaka, S.; Yamashita, Y. *J. Am. Chem. Soc.* **1995**, *117*, 6791.

(18) Havinga, E. E.; ten Hoeve, W.; Wynberg, H. *Polym. Bull.* **1991**, *29*, 119. Havinga, E. E.; ten Hoeve, W.; Wynberg, H. *Synth. Met.* **1993**, *55*−*57*, 299.

(19) Pulay, P.; Fogarasi, G. *J. Am. Chem. Soc.* **1983**, *105*, 7037.

(20) (a) Scott, A. P.; Radom, L. *J. Phys. Chem.* **1996**, *100*, 16502. (b) Rauhut, G.; Pulay, P. *J. Phys. Chem.* **1995**, *99*, 3093.

(21) Becke, A. D. *J. Chem. Phys.* **1993**, *98*, 5648.

(22) Francl, M. M.; Pietro, W. J.; Hehre, W. J.; Binkley, J. S.; Gordon, M. S.; Defrees D. J.; Pople, J. A. *J. Chem. Phys.* **1982**, *77*, 3654.

(23) Gross, E. K. U.; Kohn, W. *Adv. Quantum Chem.* **1990**, *21*, 255. *Density Functional Theory*; Gross, E. K. U., Ullrich, C. A., Gossmann, U. J., Driezler R. M., Eds.; Plenum Press: New York, 1995. *Recent Advances in Density Functional Methods, Part I*; Casida, M. E., Chong, D. P., Eds.; World Scientific: Singapore, 1995.

(24) Frisch, M. J.; Trucks, G. W.; Schlegel, H. B.; Scuseria, G. E.; Robb, M. A.; Cheeseman, J. R.; Zakrzewski, V. G.; Montgomery, J. A.; Stratman, R. E.; Burant, S.; Dapprich, J. M.; Millam, J. M.; Daniels, A. D.; Kudin, K. N.; Strain, M. C.; Farkas, O.; Tomasi, J.; Barone, V.; Cossi, M.; Cammi, R.; Mennucci, B.; Pomelli, C.; Adamo, C.; Clifford, S.; Ochterski, G.; Petersson, A.; Ayala, P. Y.; Cui, Q.; Morokuma, K.; Malick, D. K.; Rabuck, A. D.; Raghavachari, K.; Foresman, J. B.; Cioslowski, J.; Ortiz, J. V.; Stefanov, B. B.; Liu, G.; Liashenko, A.; Piskorz, I.; Komaromi, I.; Gomperts, R.; Martin, R. L.; Fox, D. J.; Keith, T.; Al-Laham, M. A.; Peng, C. Y.; Manayakkara, A.; Gonzalez, C.; Challacombe, M.; Gill, P. M. W.; Johnson, B. G.; Chen, W.; Wong, M. W.; Andres, J. L.; Head-Gordon, M.; Replogle, E. S.; Pople, J. A. *Gaussian 98*, revision A.7; Gaussian Inc.: Pittsburgh, PA, 1998.

(25) Schleyer, P. v. R.; Maerker, C.; Dransfeld, A.; Jiao, H.; van Eikema Hommes, N. J. R. *J. Am. Chem. Soc.* **1996**, *118*, 6317. Zywietz, T. K.; Schleyer, P. v. R.; Meijere, A. *J. Org. Chem.* **1998**, *63*, 3417.

(26) NICS values have been calculated using the GIAO method (Wolinski, K.; Hilton, J. F.; Pulay, P. *J. Am. Chem. Soc.* **1990**, *112*, 8251) at the B3LYP/6-311+G(2d,p) level. These data are considered only at the six-member ring centers which are determined by the nonweighted mean of the heavy atom coordinates. The calculations were carried out for the

neutral *syn*-DThNDT and *anti*-DThNDT and for the radical cation and anion of *anti*-DThNDT.

(27) Horovitz, B. *Phys. Rev. Lett*. **1981**, *47*, 1491. Horovitz, B. *Solid State Commun*. **1982**, *41*, 729.

(28) Castiglioni, C.; Lopez Navarrete, J. T.; Gussoni, M.; Zerbi, G. *Solid State Commun.* **1988**, *65*, 625. Zerbi, G.; Castiglioni, C.; Lopez Navarrete, J. T.; Tian, B.; Gussoni, M. *Synth. Met.* **1989**, *28*, D359.

(29) Casado, J.; Hernandez, V.; Hotta, S.; Lopez Navarrete, J. T. *J. Chem. Phys.* **1998**, *109*, 10419. Casado, J.; Hernandez, V.; Hotta, S.; Lopez Navarrete, J. T. *Adv. Mater*. **1998**, *10*, 1458.

(30) Hernandez, V.; Casado, J.; Ramirez, F. J.; Zotti, G.; Hotta, S.; Lopez Navarrete, J. T. *J. Chem. Phys.* **1996**, *104*, 9271. Moreno Castro, C.; Ruiz Delgado, M. C.; Hernández, V.; Hotta, S.; Casado, J.; López Navarrete, J. T. *J. Chem. Phys.* **2002**, *116*, 10419.